To appear in *Molecular Physics*
Vol. 00, No. 00, Month 200x, 1–14

SPECIAL ISSUE PAPER

Structure and dynamics of coupled viscous liquids

Andrea Ninarello, Ludovic Berthier, Daniele Coslovich

Laboratoire Charles Coulomb UMR 5221, Université de Montpellier and CNRS, Montpellier, France

(*"received"*)

We perform Monte-Carlo simulations to analyse the structure and microscopic dynamics of a viscous Lennard-Jones liquid coupled to a quenched reference configuration of the same liquid. The coupling between the two replicas is introduced via a field ε conjugate to the overlap Q between the two particle configurations. This allows us to study the evolution of various static and dynamic correlation functions across the (ε, T) equilibrium phase diagram. As the temperature is decreased, we identify increasingly marked precursors of a first-order phase transition between a low-Q and a high-Q phase induced by the field ε. We show in particular that both static and dynamic susceptibilities have a maximum at a temperature-dependent value of the coupling field, which defines a 'Widom line'. We also show that, in the high-overlap regime, diffusion and structural relaxation are strongly decoupled because single particle motion mostly occurs via discrete hopping on the sites defined by the reference configuration. These results, obtained using conventional numerical tools, provide encouraging signs that an equilibrium phase transition exists in coupled viscous liquids, but also demonstrate that important numerical challenges must be overcome to obtain more conclusive numerical evidence.

Keywords: Glass transition, structure of liquids, dynamic correlation functions.

1. Introduction

'Cloning' or 'replicating' configurations in glassy systems has a long history, which parallels the use of replica calculations to deal with systems defined by interactions containing quenched disorder [1], such as spin glasses or disordered ferromagnets [1, 2]. The relevance of replicas in the context of the glass transition of supercooled liquids has emerged more recently, and it originates from the proposal that disordered spin glass models and supercooled liquids belong to a unique universality class and undergo at low temperature a random first order transition (RFOT) between a liquid phase and an ideal glass phase [3]. Whereas this identification holds rigorously at the mean-field level [4], much remains to be understood regarding the applicability of these concepts in finite dimensions, where a variety of fluctuation effects could drastically modify the mean-field picture [5].

In recent years, it has been realized that the relevance of the RFOT construction can be assessed using 'extended' phase diagrams, where an additional control parameter is introduced to probe the RFOT physics in temperature regimes that are more easily accessible to simulations and experiments. The general idea is that precursors of the putative thermodynamic glass transition develop as the temperature is lowered in a bulk liquid, the glass phase being 'metastable' with respect to the liquid phase [6]. Therefore, the addition of well-chosen external fields could potentially stabilize this phase at temperatures well above the equilibrium glass transition and induce equilibrium phase transitions which are direct byproducts of the RFOT physics. In other words, external constraints might reveal growing

ISSN: 0040-5167 print/ISSN 1754-2278 online

DOI: 10.1080/0040516YYxxxxxxxx
http://www.informaworld.com

structural correlations characterizing viscous liquids approaching the glass transition in a way that is not accessible to the standard tools used for simple liquids [7]. Studying constrained systems thus might be useful to reveal information about bulk systems, and constrained phase transitions may exist even in systems where no finite temperature Kauzmann transition exists [8], the two issues being logically independent. Among the possible choices for such external constraints, the idea of pinning the position of a set of particles has received considerable attention recently [9, 10], in a variety of geometries [11] from finite cavities [12–14], to fully random pinning [15–21] or amorphous walls [22, 23].

In this article, we analyse the case where an external coupling to a quenched reference configuration is introduced via a field ε conjugate to the overlap Q between the two copies of the system. This situation has been studied analytically in mean-field models [6, 17, 24–26] and finite dimensional liquids [27], and it was also studied in computer simulations [27–31]. The 'annealed' situation where the coupling is between two evolving copies of the system has also received attention from a number of groups [24, 30, 32–36]. For the quenched coupling of interest in this work, the phase diagram in the (ε, T) plane has been established in the mean-field approximation [6]. In that case, an ordinary first-order transition line emerges from the bulk glass transition temperature, which separates a low-overlap (uncorrelated) phase from a large-overlap (localized) phase. This first-order transition line ends at a second-order critical point which, if present, should be in the same universality class as the random field Ising model [24, 25].

Our central goal is to use standard computational tools to explore the high-temperature region of the (ε, T) phase diagram where conventional Monte-Carlo simulations are sufficient to achieve thermalization of the coupled system. By analysing several static and dynamic correlation functions, we find a number of distinctive precursors of the first-order transition line, which allow us to define a 'Widom line' for our system. We also find that the microscopic dynamics in the high-overlap regime is markedly different from the one of bulk supercooled liquids, because single particle motion occurs mostly via spatially uncorrelated, discrete hopping on the sites defined by the reference configuration. Because this diffusion process is very slow, we conclude that an equilibrium exploration of the two phases of the model at lower temperatures is impossible using conventional means.

Our paper is organised as follows. In Sec. 2 we briefly present the model and our numerical methods. In Sec. 3 we analyse the static properties of the model, whereas Sec. 4 presents results for dynamic correlation functions. Sec. 5 closes the paper with some perspectives for future work.

2. Model and numerical methods

We performed Monte-Carlo simulations [37] of the Kob-Andersen glass-forming model [38], which is a 80 : 20 binary mixture of particles interacting via the Lennard-Jones potential

$$v_{\alpha\beta}(r) = 4\epsilon_{\alpha\beta}\left[\left(\frac{\sigma_{\alpha\beta}}{r}\right)^{12} - \left(\frac{\sigma_{\alpha\beta}}{r}\right)^{6}\right]. \quad (1)$$

where $\alpha, \beta = \{A, B\}$ denote the particles' species. The potential is shifted to ensure its continuity at the cut-off distance $r_c = 2.5$. In the following, all quantities will be expressed in reduced units, selecting ϵ_{AA} and σ_{AA} as units of energy and distance, respectively, and the Boltzmann constant is $k_B = 1$. The interaction parameters are $\sigma_{AA} = 1.0$, $\sigma_{AB} = 0.8$, $\sigma_{BB} = 0.88$, $\epsilon_{AA} = 1.0$, $\epsilon_{AB} = 1.5$ and $\epsilon_{BB} = 0.5$.

They have been chosen to prevent the mixture from crystallizing at high densities and low temperatures. We have studied this particular model because it is a well-studied and well-characterized glass-forming system [37–39]. Exploratory runs performed using molecular dynamics methods instead of Monte-Carlo suggest that the dynamical results that we report do not depend qualitatively on the specific choice of a microscopic dynamics.

We studied a system of $N = 1000$ particles in each copy. We work in three spatial dimensions using periodic boundary conditions at a number density $\rho = N/V = 1.2$, where V is the volume of the simulation box. In our Monte-Carlo simulations, we perform sequential single particle displacements by drawing random displacements within a cube of linear size $\Delta r_{\max}$ centered on the particle's position. The proposed displacement is accepted according to the Metropolis criterion. We chose $\Delta r_{\max} = 0.12$, which maximizes the diffusion constant of the system in the unconstrained mixture at $T = 1.0$, which represents the onset temperature for the bulk Lennard-Jones system. The time unit in our Monte-Carlo simulations is defined as N attempts to move a particle.

To study the coupled system, we first define the overlap Q_{12} between two configurations, 1 and 2, as

$$Q_{12} = \frac{1}{N} \sum_{i,j} \theta(a - |\mathbf{r}_{1,i} - \mathbf{r}_{2,i}|), \tag{2}$$

where $\theta(x)$ is the Heavyside function, $a = 0.3$ is a coarse-graining distance for comparing the density profiles, and $\mathbf{r}_{\alpha,i}$ denotes the position of particle i in the copy $\alpha \in \{1, 2\}$.

Our numerical procedure to study the coupled glassy problem is to draw a series of equilibrium configurations $\{\mathbf{r}_1\}$ at temperature T_1, which serve as reference configurations. We then study a second copy of the system, $\{\mathbf{r}_2\}$, which evolves at temperature T_2 and is coupled to a given reference configuration via a field ε conjugate to the overlap between the two configurations. Only the second copy is allowed to evolve in this step. The total Hamiltonian thus reads

$$H_{\{\mathbf{r}_1\}}(\{\mathbf{r}_2\}) = H_{\mathrm{LJ}}(\{\mathbf{r}_2\}) - \varepsilon Q_{12}, \tag{3}$$

where

$$H_{\mathrm{LJ}}(\{\mathbf{r}\}) = \frac{1}{2} \sum_{\alpha,\beta} \sum_{i=1}^{N_\alpha} \sum_{j=1}^{N_\beta} v_{\alpha\beta}(\mathbf{r}_{ij}) \tag{4}$$

denotes the Lennard-Jones Hamiltonian for a single copy $\{\mathbf{r}\}$, and $\varepsilon > 0$ biases the coupled system towards higher values of the overlap. In our study, we use equal temperatures for the quenched reference configurations and the system under study, $T_1 = T_2 = T$, although other choices are possible [6, 31]. The Hamiltonian (3) contains quenched disorder, because the positions of all particles in copy 1, $\{\mathbf{r}_1\}$, are held fixed. Therefore, after thermal average is performed at temperature T for a given realisation of the disorder, we need to perform an average over independent configurations of the quenched copy. We found that the disorder average plays a negligible role for the system size and the temperature range studied in this work. Therefore, we only needed to average over a small number of independent quenched configurations to obtain accurate static and dynamic properties of the system. A much more demanding disorder averaging procedure would be needed at lower temperatures [30, 31].

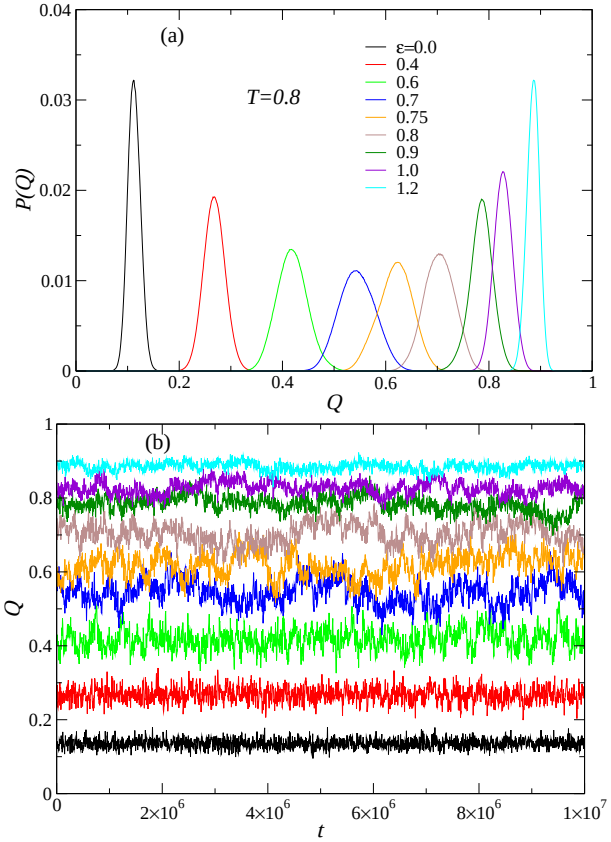

Figure 1. (a) Probability distribution of the overlap $P(Q)$ at several ε values along the isotherm $T = 0.8$. (b) Typical time series of the overlap $Q(t)$ for the same parameters (the bulk alpha-relaxation time at $T = 0.8$ is about $\tau \approx 2 \cdot 10^3$). The overlap fluctuations are broader and slower near $\epsilon^* \approx 0.7$.

Finally we find that thermalising the constrained system defined by the Hamiltonian (3) becomes increasingly difficult when ε is large and/or temperature is low. For a given state point defined by (ε, T), we consider that a system is equilibrated if the two following criteria are met. First, we require that the average of the overlap evaluated over a time window of the order of 10^5, displays no systematic drift. Second, we require that particles move an average distance of about 3 particle diameters. These empirical criteria are chosen so that both single particle dynamics and overlap fluctuations are accurately sampled in our simulations. Remark that even when the overlap value is large and the system explores a limited part of the configurational part close to the reference configuration, it is important to perform very long simulations to ensure that both static and dynamic quantities are probed accurately. As a consequence, we have not been able to study meaningful parts of the (ε, T) phase diagram for temperatures below $T = 0.7$ (our data at $T = 0.6$ barely satisfy our criteria). Note that this temperature only represents a modest degree of supercooling for the unconstrained system and is far above the mode-coupling temperature $T_{\rm mct} \approx 0.435$, but this already represents a challenging situation for the coupled system.

3. Static properties

We start by studying the static properties of the system defined by Hamiltonian (3), varying ε and T. Intuitively, we expect that large values of ε will localize the particles close to the sites defined by the position of the particles in the quenched reference configuration in order to increase the overlap Q between the two replicas.

In Fig. 1(a), we show the probability distribution of the overlap, $P(Q)$, along the representative isotherm $T = 0.8$ for increasing values of the coupling field ε. This temperature is slightly below the onset temperature ($T \approx 1.0$) of slow dynamics in the unconstrained system with $\varepsilon = 0$. As the coupling ε increases, we find indeed that $P(Q)$ becomes centered around increasingly larger values of Q. As discussed in Sec. 1, we may expect that the system undergoes a first-order phase transition between a low-Q phase and a high-Q phase when temperature is low enough. Clearly, the data in Fig. 1(a) show that the overlap increases smoothly with ε at this temperature and the phase transition, if present, must occur at lower temperatures.

However, we notice that the distributions are narrow for both small and large values of ε but broaden considerably at intermediate values corresponding to intermediate overlap values, $Q \approx 0.5$. Such a broadening of the distributions for intermediate values of ε is consistent with the idea that the system approaches the critical temperature from above.

A confirmation of this intuition is shown in Fig. 1(b) which illustrates the typical time evolution of the order parameter $Q(t)$ in the course of the Monte-Carlo simulations. We observe that the overlap displays slow fluctuations of large amplitude for intermediate values of ε, whereas temporal correlations and large excursions are strongly suppressed when the replicas are strongly coupled in the high-Q regime, or nearly uncorrelated at low ε. These qualitative observations suggest that the dynamics of the coupled system display a non-trivial variation as a function of the coupling. The large fluctuations of the global overlap Q represent a first source of dynamic slowing down for the coupled system, which we interpret as a form of critical slowing down, expected in the vicinity of a second-order critical point. Notice that the time series shown in Fig. 1 cover a window of about 10^7 timesteps, whereas the bulk alpha-relaxation time of the unconstrained system at the same temperature is $\tau \approx 2 \cdot 10^3$, which already demonstrates that accessing the properties of the coupled system in conventional numerical simulation is challenging, even at temperatures far above the critical point.

In Fig. 2(a) we show the average overlap $\langle Q \rangle$ as a function of ε for all studied temperatures, where the moments of the distribution are defined as

$$\langle Q^n \rangle = \int_0^1 dQ P(Q) Q^n. \tag{5}$$

We find that the coupling needed to localize the system in the high-overlap regime decreases rapidly upon decreasing the temperature. This directly implies that the thermodynamic driving force which allows the system to escape from a randomly chosen reference configuration also decreases with the temperature. This observation is at the core of the RFOT description of the glass transition [3].

Moreover, we observe that the crossover from the low-Q regime to the high-Q one becomes sharper and better defined as T decreases. This is again consistent with the approach to a first-order phase transition separating a normal, low-Q phase and a localized, high-Q phase. To identify this crossover more precisely, we evaluate the overlap susceptibility,

$$\chi = N[\langle Q^2 \rangle - \langle Q \rangle^2]. \tag{6}$$

The results are shown in Fig. 2(b). For each studied temperature, χ displays a well-defined maximum at a coupling $\varepsilon^* = \varepsilon^*(T)$, which we identify as the location of the crossover. The locus of $\varepsilon^*(T)$ in the (ε, T) plane represents the equivalent

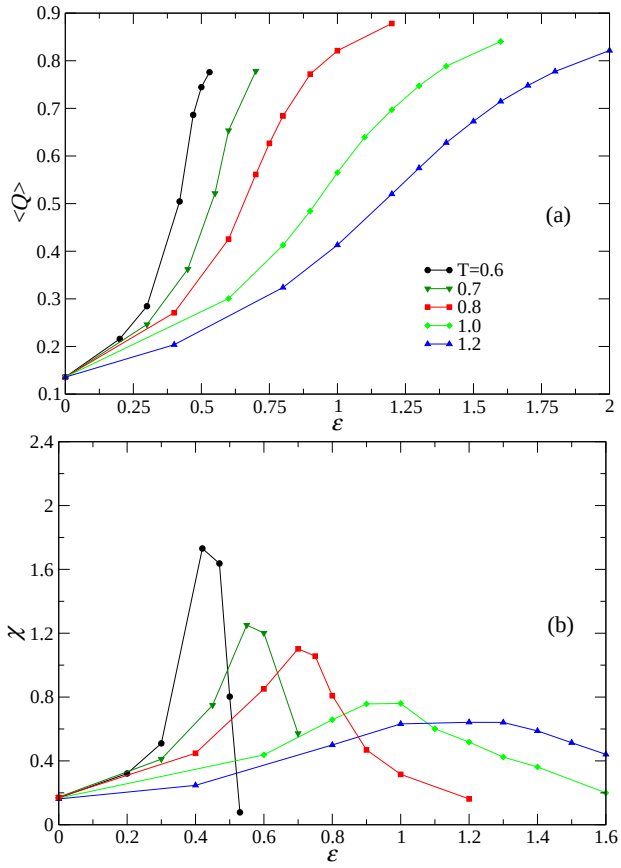

Figure 2. (a) Average overlap $\langle Q \rangle$ and (b) overlap susceptibility χ as a function of ε for various temperatures. The crossover from uncorrelated to localized regimes occurs at lower ε when T decreases, and becomes sharper.

of the Widom line [40] for conventional phase transitions, as it represents the continuation of the transition line above the critical point. It should be clear that our interpretations are consistent with the mean-field calculations, but that our numerical results do not establish that an equilibrium phase transitions actually exists for this system. An alternative view is that the clear crossover line that we detect remains a smooth crossover at any finite temperatures [19]. Deciding which is the correct scenario is beyond the scope of the present work.

The coupling parameter ε in the Hamiltonian, Eq. (3), allows one to bias the system towards higher values of the overlap Q. The small value $a = 0.3$ used to evaluate the overlap leads to the formation of 'dimers' formed when a particle in the liquid is localized close to a particle in the reference configuration. We note that higher order clusters (such as trimers) have an enormous energy cost in the studied range of temperatures and couplings, and do not form. To investigate this point more quantitatively, we have evaluated the radial distribution functions between quenched and liquid replicas at various T and ε,

$$g_{\alpha\beta}(r) = \frac{1}{VN_\alpha N_\beta} \sum_{i=1}^{N_\alpha} \sum_{j=1}^{N_\beta} \delta(r - |\mathbf{r}_{1,j} - \mathbf{r}_{2,i}|). \tag{7}$$

In Fig. 3(a) we show the radial distribution function between the large particles in the two copies, while Fig. 3(b) shows correlations between large particles in the liquid and small particles in the reference configuration. As ε increases, a well-defined peak develops near $r \approx 0$, which quantifies the increasing localisation of

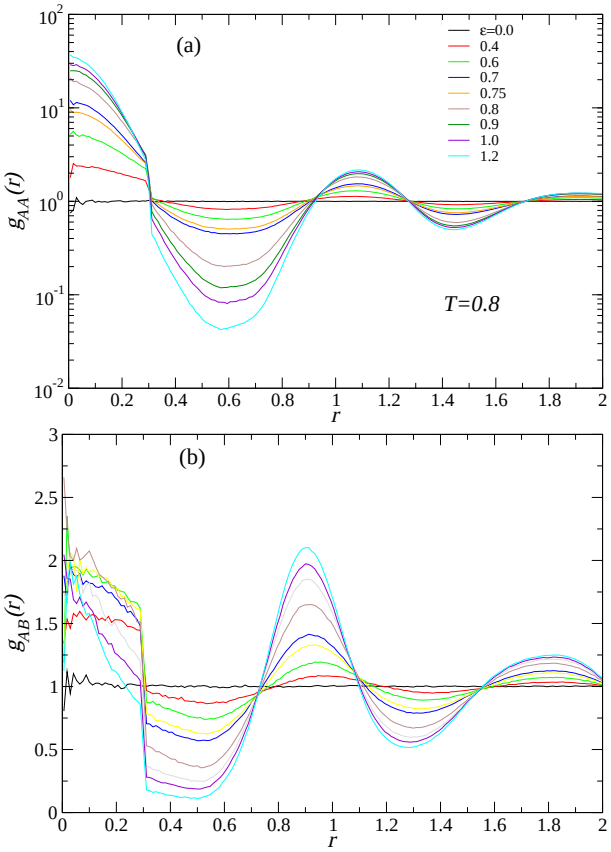

Figure 3. Radial distribution functions between quanched and fluid replicas $g_{AA}(r)$ and $g_{AB}(r)$, see Eq. (7). Both functions develop a clear maximum near $r = 0$ as ε increases, reflecting the global increase of the overlap via the formation of 'dimers'. Whereas the probability to form AA dimers increases with ε, AB dimers are more numerous near $\varepsilon^* \approx 0.7$, but are suppressed at larger coupling.

particles near the sites defined by the reference configuration. The global overlap Q is in fact directly related to the area under these peaks, and the pair correlation functions shown in Fig. 3 are the natural outcomes of integral equation approaches for the problem of coupled glassy systems [27, 32]. The pair correlation functions develop a clear minimum near $r \approx 0.6$, indicating the formation of tight dimers of liquid and quenched particles. This phenomenon resembles the formation of clusters in suspensions of neutral [41] and charged [42] ultrasoft colloidal particles. Finally, we note that the kink at $r = a$ is a direct result of the Heavyside function used to couple the two replicas and would be absent if a smoother coupling (for instance a Gaussian function) had been used.

The comparison between $g_{AA}(r)$ and $g_{AB}(r)$ shows that the peaks at short distance in these functions behave somewhat differently. First, the overall amplitude of the two peaks is very different, as testified by the different vertical scales used to represent these two functions in Fig. 3 (the amplitude at $r = 0$ is about 10 times larger for AA than for AB pairs). This shows that particles in the liquid replica tend to localize to a site of the reference configuration occupied by a particle of the same type when the coupling is strong, although the probability to form 'defective' AB dimers is not negligible. A more careful analysis of the peaks also shows that the peak amplitude in g_{AA} increases monotonically with ε whereas the one in g_{AB} is maximum near the crossover value $\varepsilon^* \approx 0.7$. This observation suggests that the large fluctuations of the overlap revealed in Fig. 1 when $\varepsilon \approx \varepsilon^*$ likely correspond to a large variety of localized configurations, where dimers of various kinds can be formed. When the coupling becomes stronger, the system resembles increasingly to the reference configuration and AB dimers are suppressed, at the expense of

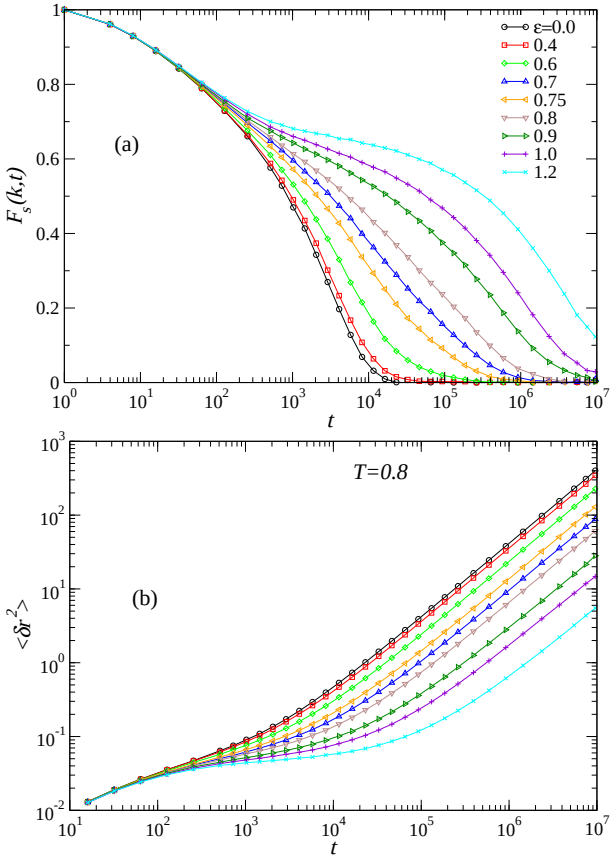

Figure 4. (a) Self-part of the intermediate scattering function $F_s(k,t)$ evaluated at $k = 7.4$ along the isotherm $T = 0.8$ and various ε coupling values. (b) Mean-squared displacement $\delta r^2(t)$ for the same state points. The single particle dynamics slows down monotonically by increasing ε, revealing the increasing localisation of the particles.

AA and BB dimers. Indeed, we find that $g_{BB}(r)$ essentially tracks the behaviour of $g_{AA}(r)$. The conclusions are also supported by the decomposition of the global overlap into contributions coming from the various species.

4. Microscopic dynamics

Close inspection of the time series of the overlap in Fig. 1(b) suggests that the dynamics of the liquid replica becomes increasingly sluggish upon increasing the coupling. In the previous section, we (tentatively) attributed this slowing down to the crossing of a Widom line where overlap fluctuations are very broad. However, we also noticed that dimers of like-particles form with increasing coupling, which corresponds to an increasing localization of the liquid particles on the quenched sites defined by the reference configuration. In this section, we will show that this localisation dramatically impacts the available relaxation pathways.

To characterize the single-particle dynamics of the liquid replica, we evaluate the self-part of the intermediate scattering function

$$F_s(k,t) = \frac{1}{N}\left\langle \sum_i \exp[i\mathbf{k}\cdot(\mathbf{r}_i(t) - \mathbf{r}_i(0)] \right\rangle, \tag{8}$$

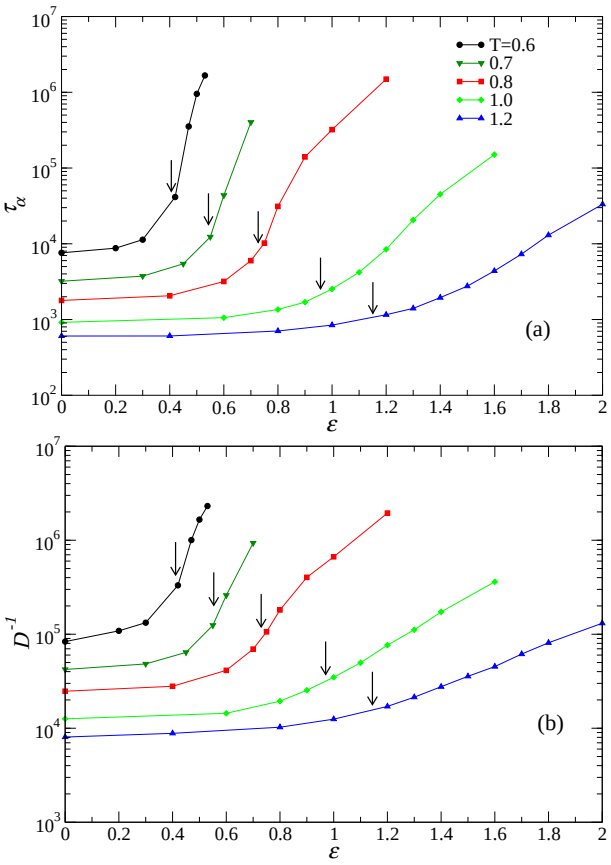

Figure 5. Evolution of the (a) structural relaxation times τ_α and of (b) the diffusion coefficients D for large particles as a function of ε for different temperatures. The dynamics slows down dramatically when the crossover $\varepsilon^*(T)$ (shown with arrows) is crossed. Note that the change in τ_α and D^{-1} is quantitatively different, as demonstrated in Fig. 6.

and the mean-squared displacement

$$\delta r^2(t) = \frac{1}{N} \left\langle \sum_i |\mathbf{r}_i(t) - \mathbf{r}_i(0)|^2 \right\rangle . \tag{9}$$

Both time correlation functions are evaluated for the large A particles (the majority species) along the representative isotherm $T = 0.8$. The results are displayed in Fig. 4.

The unconstrained system displays practically no caging at this temperature, in agreement with the results of Ref. [37] on the Monte-Carlo dynamics of the same model. Upon increasing ε, however, the dynamics slows down significantly. The relaxation of $F_s(k,t)$ at long times becomes increasingly stretched and eventually develops a clear plateau at intermediate times for the highest values of ε. A similar plateau is observed in the mean-squared displacement $\delta r^2(t)$. A comparison of the mean squared displacement for A and B particles (not shown here) reveals that in the high-Q regime, the smaller B particles are somewhat less strongly localized on the quenched sites and can flow more easily than the large particles. The distinct dynamics between large and small particles is also observed in the bulk system at low temperatures [38].

As usual, we define the structural relaxation times τ_α from the condition $F_s(k,\tau_\alpha) = 1/e$ and the diffusion coefficients D from the Einstein relation $\lim_{t\to\infty} \delta r^2(r) = 6Dt$. In Fig. 5 we show the ε-dependence of τ_α and D^{-1} for A particles. For each studied temperature, we observe a marked increase of both

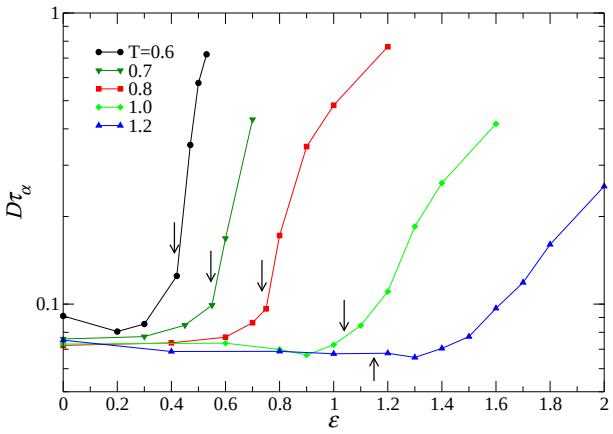

Figure 6. Decoupling of the diffusion constant and the structural relaxation is established since the product $D\tau_\alpha$ increases dramatically with ε. The arrows mark the crossover $\varepsilon^*(T)$.

τ_α and D^{-1} as the coupling approaches the crossover value ε^*, determined from the analysis of the overlap susceptibility (see Sec. 3). Upon further increasing ε, both quantities continue to increase steadily, and the single particle dynamics slows down dramatically. Note that all data points in Fig. 5 are fully equilibrated according to the criteria detailed in Sec. 2.

An inspection of Fig. 5 suggests that diffusion and structural relaxation both slow down dramatically in the high-Q regime, but their behaviour is also strongly decoupled, as D^{-1} appears to change less than τ_α. This is demonstrated more clearly in Fig. 6, where we show the product $D\tau_\alpha$ for the A particles. We observe that $D\tau_\alpha$ remains constant until ε reaches ε^*, above which it starts to grow significantly. Interestingly, the deviation is visible for both species, but it is less pronounced for the small particles (not shown).

Such violation of the Stokes-Einstein relation, $D\tau_\alpha \approx D\eta \sim cst$, is expected in systems whose dynamics is highly heterogeneous, such as supercooled liquids [43], although other sources of decoupling have been identified in simple fluids [44]. The coexistence of slow and fast particles in the sample leads to a decoupling between τ_α and D, because the former is mostly dominated by the slow particles, whereas the latter is dominated by the fast ones. We remark, however, that the Stokes-Einstein violation at large ε is more pronounced than the one observed by decreasing temperature in the unconstrained model. This suggests that the physical origin of this decoupling might be somewhat different in the constrained model than in the bulk.

A first hypothesis to explain the decoupling is the existence of large-scale spatial correlations in the dynamics [45]. This hypothesis is reasonable, since static correlations are promoted by the coupling field ε, as testified by the maximum in the static susceptibility χ in Fig. 2.

To quantify spatially heterogeneous dynamics in a more precise manner, we evaluate the four-point dynamic susceptibility [46–48],

$$\chi_4(t) = N\left[\langle f_s(k,t)^2\rangle - \langle f_s(k,t)\rangle^2\right], \tag{10}$$

where $f_s(k,t) = \frac{1}{N}\sum_i \exp[i\mathbf{k}\cdot(\mathbf{r}_i(t) - \mathbf{r}_i(0))]$ represents the instantaneous value of the self-intermediate scattering function. In supercooled liquids, $\chi_4(t)$ is characterized by a single peak, located around τ_α, whose height χ_4^* provides a simple measure of the degree of heterogeneity of the dynamics (it scales roughly as the dynamic correlation volume). We find that the constrained system displays similar peaks in $\chi_4(t)$, and we represent the variation of χ_4^* as a function of ε in Figure 7

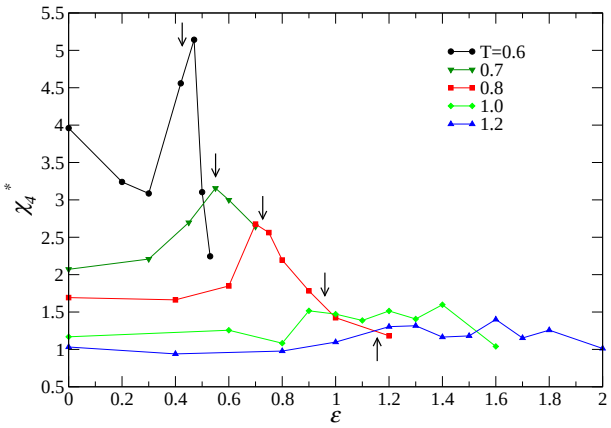

Figure 7. Evolution of the maximum of the four-point dynamic susceptibility χ_4^* as a function of ε. Spatial correlations are maximum near the static crossover $\varepsilon^*(T)$ (indicated by arrows).

for all studied temperatures.

At high temperature, χ_4^* is essentially constant and practically independent of ε. When $T < 1.0$ the behavior changes and χ_4^* varies non-monotonically as a function of ε, with a maximum located very close to the crossover coupling ε^* defined from the maximum of the static overlap fluctuations. This shows that spatial correlations in the dynamics are essentially slaved to the spatial fluctuations of the static overlap. In particular, we find that χ_4^* decreases rapidly as ε is increased beyond $\varepsilon^*(T)$. This implies that the collective dynamics in the localized regime is actually strongly suppressed and that particles move instead in a spatially uncorrelated manner. Therefore, the strong decoupling reported in Fig. 6 does not stem from the coexistence of dynamically correlated domains.

Nevertheless, it is interesting to note that the behaviour of the static and dynamic susceptibilities χ and χ_4 is similar only when ε is large, but it differs dramatically when $\varepsilon \to 0$ where dynamic fluctuations increase rapidly as T decreases whereas static ones are essentially independent of temperature for the unconstrained system at $\varepsilon = 0$. The fact that static and dynamic fluctuations have distinct temperature dependences in the moderately supercooled regime was noted before [11, 15, 22].

A final notable feature of our data is observed at the lowest studied temperature at $T = 0.6$ in Fig. 7. Despite the limited dynamic range we can access, the data reveal an additional feature, since χ_4^* is a decreasing function of ε at small ε. Such a decrease of χ_4^* is reminiscent of the one observed with randomly pinned particles [20, 49]. For such systems, the relevant order parameter is the concentration of pinned particles, which plays an analogous role to the coupling ε in the present model. In the randomly pinned systems, however, there was no trace of a subsequent increase of χ_4^* as a function of the concentration of pinned particles [20], presumably because the crossover line cannot be easily approached in the time window available to conventional computer simulations in the case of random pinning.

The analysis of the four-point dynamic susceptibility shows that the particle dynamics becomes essentially uncorrelated in the high-overlap regime. Therefore, the explanation of the strong decoupling behavior between diffusion and alpha-relaxation time should be sought in the properties of single particle motion. To elucidate this aspect, we evalute the self-part of the van-Hove correlation function,

$$G_s(r,t) = \left\langle \sum_i \delta(r - |\mathbf{r}_i(t) - \mathbf{r}_i(0)|) \right\rangle . \tag{11}$$

In Fig. 8, we show the evolution of the distribution of single particle displacements

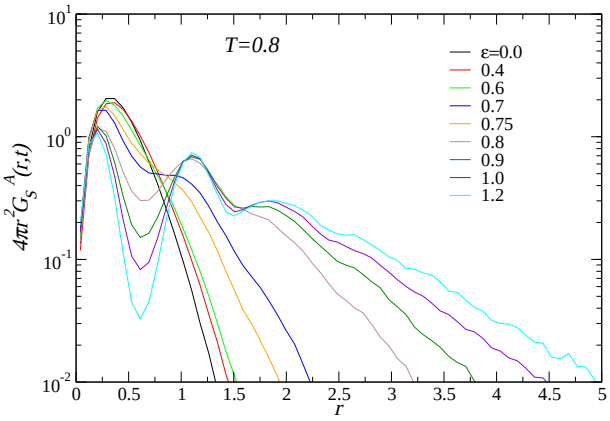

Figure 8. Self-part of the van-Hove correlation function $4\pi r^2 G_s(r,t)$ for large particles for several ε at $T = 0.8$. The distributions are evaluated at times t such that $F_s(k,t) = 0.2$. They broaden considerably as ε increases, and the tails develop a multi-peak structure resulting from discrete particle hopping.

for increasing ε, adjusting for each value of ε the timescale such that $F_s(k,t) \approx 0.2$ (this allows us to probe displacements that are large enough to better reveal the structure of the van-Hove function). The distributions of displacements are essentially featureless and close to a Gaussian for small ε, but they broaden considerably when $\varepsilon > \varepsilon^*(T)$. This considerable broadening suggests that at any given time, the system is composed of fast-moving and slow-moving particles that coexist in space. This feature alone is sufficient to account quantitatively for a strong decoupling phenomenon [50]. It is interesting to note that the coexistence in space of fast and slow particles with increasingly heterogeneous dynamics is not associated to growing spatial correlations of the dynamic relaxation; this is instead a purely local phenomenon.

The data in Fig. 8 not only show that the distributions broaden with ε, since the shape of the distributions is also changing qualitatively. The distributions are strongly non-Gaussian at large ε, and the emergence of secondary peaks is also obvious. These peaks suggest that the particle dynamics evolves from a continuous diffusive process at small ε, to a slow, intermittent, hopping process at large ε. Physically, this means that particles jump mostly from one site to another, where the 'sites' are defined by the positions of the particles in the reference configuration. This interpretation is harmonious with the observation of the formation of dimers discussed in Sec. 3. Finally, we note that particles of both species are involved in the hops, although the behaviour seems less pronounced for small particles, whose van-Hove functions are less structured than for large particles (data not shown). This observation contrasts with the behavior of the unconstrained model at low temperatures around $T_{\rm mct}$, where the jump dynamics mostly involve the smaller B particles.

5. Conclusions

We have used conventional Monte-Carlo simulations to study a viscous liquid coupled to a frozen reference configuration of the same liquid at the same temperature. Our exploration of the high-temperature portion of the (ε, T) phase diagram reveals a 'Widom line' of thermodynamic and dynamic anomalies signalling the crossover from an uncorrelated liquid regime to a localized one, in which particles of the system are strongly constrained to reside near the sites of the reference configuration. These results as compatible with the existence of a line of first-order transitions at lower temperature terminating at a second-order critical point. Our results show

that computational approaches to this problem suffer from two distinct sources of dynamic slowing down. First, as in any phase transition, the order parameter (here the global overlap) displays large fluctuations near coexistence, reflecting the emergence of a non-trivial free-energy profile. Second, the single-particle motion becomes very slow in the high-overlap region because particles must hop on the sites of the reference configuration in a highly constrained manner in order for the global overlap to remain large. Altogether, this means that at least two distinct strategies need to be implemented in order to study the phase diagram at lower temperatures to overcome both the free-energy barriers near the phase transition and the slowing down of the particles motion in the high-overlap regime. Work is in progress in this direction [31], which will hopefully allow for a direct study of the equilibrium phase diagram of coupled viscous liquids.

Acknowledgements

We are very pleased and honoured to contribute an article to this Special Issue in honour of J.-P. Hansen whose work, career and integrity set an admirable example to all of us. The research leading to these results has received funding from the European Research Council under the European Union's Seventh Framework Programme (FP7/2007-2013) / ERC Grant agreement No 306845.

References

[1] M. Mézard, G. Parisi and M.A. Virasoro, *Spin Glass Theory And Beyond: An Introduction To The Replica Method And Its Applications* (World Scientific, Singapore, 1986).
[2] A.P. Young, *Spin Glasses and Random Fields* (World Scientific, Singapore, 1998).
[3] T.R. Kirkpatrick, D. Thirumalai and P.G. Wolynes, Phys. Rev. A **40**, 1045 (1989).
[4] P. Charbonneau, J. Kurchan, G. Parisi, P. Urbani and F. Zamponi, Nature Comm. **5**, 3725 (2014).
[5] L. Berthier and G. Biroli, Rev. Mod Phys. **83**, 587 (2011).
[6] S. Franz and G. Parisi, Phys. Rev. Lett. **79**, 2486 (1997).
[7] J.P. Hansen and I.R. McDonald, *Theory of Simple Liquids*, 2nd ed. (Academic Press, London, 1986).
[8] L. Foini, F. Krzakala and F. Zamponi, J. Stat. Mech. p. P06013 (2012).
[9] J.P. Bouchaud and G. Biroli, J. Chem. Phys. **121**, 7347 (2004).
[10] A. Montanari and G. Semerjian, J. Stat. Phys. **125**, 23 (2006).
[11] L. Berthier and W. Kob, Phys. Rev. E **85**, 011102 (2012).
[12] G. Biroli, J.P. Bouchaud, A. Cavagna, T.S. Grigera and P. Verrocchio, Nature Phys. **4**, 771 (2008).
[13] A. Cavagna, T.S. Grigera and P. Verrocchio, J. Chem. Phys. **136**, 204502 (2012).
[14] G.M. Hocky, T.E. Markland and D.R. Reichman, Phys. Rev. Let. **108** (22), 225506 (2012).
[15] B. Charbonneau, P. Charbonneau and G. Tarjus, Phys. Rev. Lett. **108**, 035701 (2012).
[16] W. Kob and L. Berthier, Phys. Rev. Lett. **110**, 245702 (2013).
[17] C. Cammarota and G. Biroli, J. Chem. Phys. **138**, 12A547 (2013).
[18] C. Cammarota and G. Biroli, Proc. Natl. Acad. Sci. **109**, 8850 (2012).
[19] R.L. Jack and L. Berthier, Phys. Rev. E **85**, 021120 (2012).
[20] C.J. Fullerton and R.L. Jack, Phys. Rev. Lett. **112**, 255701 (2014).
[21] M. Ozawa, W. Kob, A. Ikeda and K. Miyazaki, Equilibrium phase diagram of a randomly pinned glass-formerarXiv:1412.4911 (unpublished) 2014.
[22] W. Kob, S. Roldán-Vargas and L. Berthier, Nature Phys. **8**, 164 (2012).
[23] G.M. Hocky, L. Berthier, W. Kob and D.R. Reichman, Phys. Rev. E **89**, 052311 (2014).
[24] S. Franz and G. Parisi, J. Stat. Mech. p. P11012 (2013).
[25] G. Biroli, C. Cammarota, G. Tarjus and M. Tarzia, Phys. Rev. Lett. **112**, 175701 (2014).
[26] J. Kurchan, G. Parisi and M.A. Virasoro, J. Phys. I **3**, 1819 (1999).
[27] M. Cardenas, S. Franz and G. Parisi, J. Chem. Phys. **110**, 1726 (1999).
[28] S. Franz and G. Parisi, Physica A **261**, 317 (1998).

[29] C. Cammarota, A. Cavagna, I. Giardina, G. Gradenigo, T.S. Grigera, G. Parisi and P. Verrocchio, Phys. Rev. Lett. **105**, 055703 (2010).
[30] L. Berthier, Phys. Rev. E **88**, 022313 (2013).
[31] L. Berthier and R.L. Jack, Evidence for a disordered critical point in a glass-forming liquidarXiv:1503.08576 (unpublished) 2015.
[32] J.M. Bomont, G. Pastore and J.P. Hansen, EPL (Europhysics Letters) **105**, 36003 (2014).
[33] J.M. Bomont, J.P. Hansen and G. Pastore, J. Chem. Phys. **141**, 174505 (2014).
[34] G. Parisi and B. Seoane, Phys. Rev. E **89**, 022309 (2014).
[35] M. Mézard, Physica A **265**, 352 (1999).
[36] J.P. Garrahan, Phys. Rev. E **89**, 2014 (2014).
[37] L. Berthier and W. Kob, J. Phys.: Condens. Matter **19**, 205130 (2007).
[38] W. Kob and H.C. Andersen, Phys. Rev. E **51**, 4626 (1995).
[39] L. Berthier and D. Coslovich, Proc. Natl. Acad. Sci. USA **111**, 11668 (2014).
[40] C. Domb and M.S. Green, *Phase Transitions and Critical Phenomena. Vol. 2.* (Academic Press, London, 1972).
[41] B.M. Mladek, D. Gottwald, G. Kahl, M. Neumann and C.N. Likos, Phys. Rev. Lett. **96**, 045701 (2006).
[42] D. Coslovich, J.P. Hansen and G. Kahl, J. Chem. Phys. **134**, 244514 (2011).
[43] M.D. Ediger, Annu. Rev. Phys. Chem. **51**, 99 (2000).
[44] B. Charbonneau, P. Charbonneau, Y. Jin, G. Parisi and F. Zamponi, J. Chem. Phys. **139**, 164502 (2013).
[45] G. Tarjus and D. Kivelson, J. Chem. Phys. **103**, 3071 (1995).
[46] L. Berthier, G. Biroli, J.P. Bouchaud, W. Kob, K. Miyazaki and D.R. Reichman, J. Chem. Phys. **126**, 184503 (2007).
[47] L. Berthier, G. Biroli, J.P. Bouchaud, W. Kob, K. Miyazaki and D.R. Reichman, J. Chem. Phys. **126**, 184504 (2007).
[48] C. Toninelli, M. Wyart, L. Berthier, G. Biroli and J.P. Bouchaud, Phys. Rev. E **71**, 041505 (2005).
[49] W. Kob and D. Coslovich, Phys. Rev. E **90**, 052305 (2014).
[50] L. Berthier, D. Chandler and J.P. Garrhan, Europhys. Lett. **69**, 320 (2005).